J Solid State Electrochem (2009) 13:745–754
DOI 10.1007/s10008-008-0599-y

ORIGINAL PAPER

Electrochemical impedance study of hydrogen evolution on Bi(001) electrode in the $HClO_4$ aqueous solutions

Eneli Härk · Karmen Lust · Alar Jänes · Enn Lust

Received: 3 April 2008 / Accepted: 23 May 2008 / Published online: 25 June 2008
© Springer-Verlag 2008

Abstract Electrochemical impedance spectroscopy has been applied for investigation of the hydrogen evolution kinetics at the electrochemically polished Bi(001) plane, and the complicated reaction mechanism (slow adsorption and charge-transfer steps) has been established. The charge-transfer resistance and adsorption capacitance values depend noticeably on the electrode potential applied. The adsorption resistance is maximal in the region of electrode potential E_{min}=−0.65 V vs. (Hg|Hg_2Cl_2|4 M KCl), where the minimal values of constant phase element (CPE) coefficient Q have been calculated. The fractional exponent α_{CPE} values of the CPE close to unity ($\alpha_{CPE}\geq 0.94$ and weakly dependent on the electrode potential and pH of solution ($c_{HClO_4} \leq 2 \times 10^{-3}$ M) have been obtained, indicating the weak deviation of Bi(001)|$HClO_4$+H_2O interface from the ideally flat capacitive electrode. Q differs only very slightly from double-layer capacitance C_{dl} values in the whole region of potentials and c_{HClO_4}, investigated.

Keywords Impedance · Bismuth single crystal · Cathodic hydrogen evolution

Introduction

The various electrochemical techniques—classical polarization measurements [1–5], potential relaxation [6, 7], electrochemical impedance spectroscopy (EIS) [8, 9] and potential-step coulometry [10, 11] have been applied for analysis of the cathodic hydrogen evolution reaction (HER) at different metal electrodes. The controversial conclusions at variously pretreated polycrystalline electrodes, assuming the formation of a Pd–H layer and formation of the supersaturated region of H_2 gas in the thin solution layer at the Pt electrode|electrolyte interface, from which molecular H_2 diffuses away [9, 13, 14], have been made. The different explanations given are not surprising because the cathodic hydrogen evolution and the interaction of hydrogen atoms with Pt-metals, extensively studied using electrochemical and surface science techniques, have been found to be highly sensitive on the single-crystal plane surface structure [3–5]. The second complication is involving absorption and diffusion of hydrogen within the thin metal surface layer (almost palladium, but also rhodium, nickel, and other metals and alloys) discussed by various authors [2, 12, 14–22].

The influence of the crystallographic structure of Ni(*hkl*) electrodes has been studied [23] and it was found that the hydrogen evolution overpotential increases in the order of planes (110)<(100)<(111), i.e. with the reticular density of plane [23–25].

The detailed studies at Ag(*hkl*) and Au(*hkl*) planes [26–30] show that there is a noticeable influence of the electrode surface structure on the kinetic parameters of HER. At constant electrode potential, the electroreduction rate of H_3O^+ increases in the order of planes Ag(110)<Ag(100)<Ag(111) [27, 29]. A very weak dependence of the exchange current density j_0 on the surface structure of the Au(*hkl*) electrode has been observed, and j_0 increases in the order Au(110)<Au(100)<Au(111). The data for Au(*hkl*) planes are controversial [26, 30], explained by the strong influence of the surface reconstruction phenomenon of the Au

E. Härk · K. Lust · A. Jänes · E. Lust (✉)
Institute of Chemistry, University of Tartu,
2 Jakobi Street,
51014 Tartu, Estonia
e-mail: enn.lust@ut.ee

interface on the kinetic parameters of hydrogen evolution [24, 25, 31–33].

A very limited amount of experimental data for single-crystal planes of so-called Hg-like metals (Bi, Cd, Sb, [1, 23, 25, 34, Härk and Lust 2008, in preparation]; i.e. of metals with high hydrogen evolution overpotential [35–38]) has been performed. The discharge of hydronium ion with formation of adsorbed intermediate $H_3O^+ + e^- + M = MH_{ads} + H_2O$ is well known to be the rate-controlling step of HER at the mercury and bismuth electrodes [31, 34–38, Härk and Lust 2008, in preparation].

The noticeable influence of the crystallographic structure of the Bi(111), Bi(001), and Bi$(01\bar{1})$ single-crystal planes on the kinetic parameters of HER has been observed in the $(1-x)$M $HClO_4 + x$M $LiClO_4$ solutions (where x is the mole fraction of $LiClO_4$) [1]. The remarkable dependence of the Tafel constant, an apparent transfer coefficient α and j_0 on the Bi(hkl) surface structure, as well as on the composition of the electrolyte, has been established and discussed [1, 24, 25, Härk and Lust 2008, in preparation]. Noticeable deviation from the simplified version of the classical Frumkin discharge model, ignoring specific adsorption of reactant, intermediate particles and product [4, 35], has been observed [1]. In addition, influence of pH of the supporting electrolyte solution $(1-x)$ M $HClO_4 + x$M $LiClO_4$ on the electroreduction kinetics of the $[Co(NH_3)_6]^{3+}$ cations has been observed [34, Härk and Lust 2008, in preparation], impossible to explain taking into account that solvated protons are not involved in the molecular mechanism of the electroreduction process of the hexaamminecobalt(III) complex cations at Bi(hkl) planes.

The main aim of this work was to study the kinetics of HER at the electrochemically polished (EP) Bi(001) single-crystal plane in diluted solutions of $HClO_4$, using EIS [39–44] and classical methods, and to compare the results with those obtained by the classical Tafel overvoltage measurement method for $(1-x)$ M $HClO_4 + x$M $LiClO_4$ solutions with constant ionic strength [1]. These data are useful for the more detailed analysis of the $[Co(NH_3)_6]^{3+}$ electroreduction reaction mechanism, taking into account that simultaneous HER and $[Co(NH_3)_6]^{3+}$ electroreduction reactions probably occur on the Bi(hkl) planes at more negative potentials than the zero-charge potential [1, 24, 25, 34, Härk and Lust 2008, in preparation].

Theoretical introduction

It is generally accepted that the total current density j_t passing through the electrode|electrolyte interface consists of the non-faradic (i.e. so-called double-layer charging) j_{nf} and faradic j_f parts, and applying the ac potential perturbation $\Delta E(\omega)$, (ω is angular frequency, $\omega = 2\pi f$, where f is ac frequency) the total interfacial impedance can be expressed as

$$Z_t^{-1}(\omega) = Z_{nf}^{-1}(\omega) + Z_f^{-1}(\omega), \tag{1}$$

if ohmic potential drop $jR \approx 0$, where R is ohmic resistance. HER at high cathodic overpotentials $\eta << 0$ from the acidic aqueous solution, to a first approximation, can be characterized by the following elementary steps [1, 9, 12, 13, 17, 18, 26, 27, 30, 34–37, Härk and Lust 2008, in preparation]:

$$M + H_3O^+ + e^- \underset{k_{-1}}{\overset{k_1}{\leftrightarrow}} MH_{(ads)} + H_2O \quad \text{(Volmer reaction)} \tag{2a}$$

$$MH_{(ads)} + H_3O^+ + e^- \underset{k_{-2}}{\overset{k_2}{\leftrightarrow}} H_{2(S)} + M + H_2O \ \text{(Heyrovsky reaction)} \tag{2b}$$

where M is metal, H_3O^+ stands for solvated protons, $H_{2(S)}$ is the molecular hydrogen adsorbed at the surface and $MH_{(ads)}$ is the reaction intermediate, formed after electron transfer from metal M to solvated proton H_3O^+. k_1, k_{-1}, k_2, and k_{-2} are the rate constants of corresponding reactions. Taking into account the possible weak adsorption of reaction intermediate $MH_{(ads)}$ at the Bi electrode surface [1, 35, 36], the faradaic impedance can be mathematically simulated as Eq. (3a), if we accept the so-called model for adsorption of one intermediate particle at an electrode surface [17, 18, 28–30, 35–37]:

$$\frac{1}{Z_f} = \frac{1}{R_{ct}} + \frac{B}{j\omega + G} \tag{3a}$$

where $j = \sqrt{-1}$ and the inverse charge-transfer resistance R_{ct} is given as:

$$\frac{1}{R_{ct}} = \frac{1}{RT}[\alpha_1 k_1(1-\theta) + (1-\alpha_1)k_{-1}\theta + \alpha_2 k_2 \theta + (1-\alpha_2)k_{-2}(1-\theta)] \tag{3b}$$

$$B = \frac{1}{RT\Gamma_{max}}(-k_1 - k_{-1} + k_2 + k_{-2}) \times [\alpha_1 k_1(1-\theta) + (1-\alpha_1)k_{-1}\theta - \alpha_2 k_2 \theta - (1-\alpha_2)k_{-2}(1-\theta)] \tag{3c}$$

and

$$G = \frac{1}{\Gamma_{max}}(k_1 + k_{-1} + k_2 + k_{-2}) = \frac{F}{\sigma_1}(k_1 + k_{-1} + k_2 + k_{-2}) \tag{3d}$$

where the α_1 and α_2 are the symmetry coefficients, θ is the surface coverage and Γ_{max} is maximal Gibbs adsorption and $F\Gamma_{max} = \sigma_1$ is the charge necessary for the total surface coverage by adsorbed intermediate.

Experimental

The massive bismuth single crystal was grown by the modified Czochralski method (purity 99.99999%) at the Institute of Problems of Microelectronics Technology and Superpure Materials, Russian Academy of Sciences. The Bi(001) plane orientation was obtained using X-ray diffraction method and the disorientation angle was smaller than 0.5°. The isolation of the surface area not of interest was carried out by a thin polystyrene film prepared using the solution of polystyrene dissolved in toluene. After evaporation of toluene, the electrode was placed into a Teflon holder [1, 24, 25]. The surface was polished mechanically to mirror finish, using standard metallographic procedure and, thereafter, electrochemically in the KI+HCl aqueous solution at current density ≥1.5 $A \cdot cm^{-2}$ [1, 24, 25, 34, Härk and Lust 2008, in preparation]. After electrochemical polishing, the electrode was immediately rinsed with MilliQ+ water and submerged under constant electrode potential −0.64 V vs. $Hg|Hg_2Cl_2|4$ M KCl (4 M CE) into xM $HClO_4$ aqueous solution (x from 1×10^{-3} to 1×10^{-2} M), deaerated with the pure argon (99.9995%).

The reference 4 M KCl calomel electrode was connected to the impedance cell through the very long Luggin capillary [1, 24, 25, 34, Härk and Lust 2008, in preparation] to avoid the contamination of $HClO_4$ solution with Cl^- anions. In this paper, all electrode potentials are given vs. 4 M CE and difference with saturated calomel electrode (SCE) is 4 mV. Current density values, stabilized after at least 2 h polarization, were measured using Pine rotating electrode system. The aqueous $HClO_4$ solutions were prepared from the redistilled perchloric acid (Aldrich 99.999%) using MilliQ+ water (>18.2 M Ω cm^{-1}). The electrochemical impedance was measured at the rotating disk Bi(001) single-crystal electrodes (150 rpm) to seclude the H_2 from surface with the exposed superficial area 0.1 cm^2. For impedance measurements, the electrolytic cell with a very large polycrystalline Pt counter electrode was used (flat cross section area ~40 cm^2). Bi(001) plane has been selected out because of the very good electrochemical stability in the wide potential region [1, 34, Härk and Lust 2008, in preparation].

The electrochemical impedance data have been obtained using Autolab PGSTAT 30 with FRA2 (±5 mV modulation) within the frequency region from 0.05 to $1\cdot10^4$ Hz. The Kramers–Kronig tests have been made to select out the frequency region free from systematic errors and it has been found that the data for $c_{HClO_4} = 0.001$ M and for 0.01 M at $f \leq 2\times10^3$ Hz and $f \leq 7\times10^3$ Hz respectively, can be used for detailed kinetic analysis [18, 19, 39–43]. Based on the data presented in Figs. 1b, 2b and 3b, the provisional values of α_{CPE} can be calculated in good agreement with the data obtained from the slope of $\log(-Z'')$ vs. $\log f$ plots. It should be noted that according to some works, the impedance complex plane plots can be used in the wider high-frequency region [18, 43] adding some elements into the equivalent circuit (very high frequency R_{hf} and C_{hf} elements). However, based on the future equivalent circuit (EC) analysis, these elements (as well as an additional Pt wire electrode acting as a low impedance bypass to conventional reference electrode [18, 43]) have only very small influence on the fitting parameters for the medium and low-frequency Nyquist plot region, i.e., on the CPE fractional exponent α_{CPE} and coefficient Q, as well as R_{ad} and R_{ct} values, respectively.

Various equivalent circuits have been tested for fitting of the experimental impedance complex plane ($-Z''$ vs. Z'), Bode ($\log|Z|$ and phase angle ϕ vs. $\log f$ plots), $\log(-Z'')$ vs. $\log f$ plots using non-linear least-squares minimization program that minimizes the sum of $(Z_m - Z_c)^2$ terms for all frequency points measured (Z_m and Z_c are the measured and calculated impedance values, respectively [45, 46]). The theoretical spectrum calculated (based on the arbitrarily chosen model) has been fitted to the experimental impedance data (spectrum) and the best-fitted case has been selected on the basis of the minimal χ^2-function value. The standard deviation (SD) of the fit defined as, $SD = \sqrt{\chi^2/2l - p}$ (where l denotes the number of points and p denotes the number of parameters of the fitting model), is a general measure of the goodness of fit and therefore SD method [46] (only for ECs without distributed elements (CPE)) has been applied in this work too. Additionally, the weighted sum of squares Δ^2, as well as errors of individual parameters obtained have been analyzed [18, 20, 45, 46] keeping the number of experimental points constant for all fittings made using various equivalent circuits.

Results and discussion

Impedance spectroscopy

Impedance complex plane and Bode plots as well as $\log(-Z'')$ vs. $\log f$ plots for the Bi(001) electrode measured in various $HClO_4$ aqueous solutions (c_{HClO_4} varies from 1×10^{-3} to 1×10^{-2} M) at constant rotation velocity v=150 rpm and at various fixed electrode potentials are presented in Figs. 1, 2 and 3, where $Z''=(j\omega C_s)^{-1}$ and C_s is the series capacitance of the interface studied [18, 39–46]. Visual analysis of different kind of impedance spectra shows clearly a significant advantage of the Bode plots (Figs. 1c,d, 2c,d and 3c,d) over the impedance complex plane plots. Bode plots show clear impedance data over the total frequency range examined while the impedance complex plane data are very informative for the limited low-frequency region (f<100 Hz) but higher frequency data at high extent are screened. The log

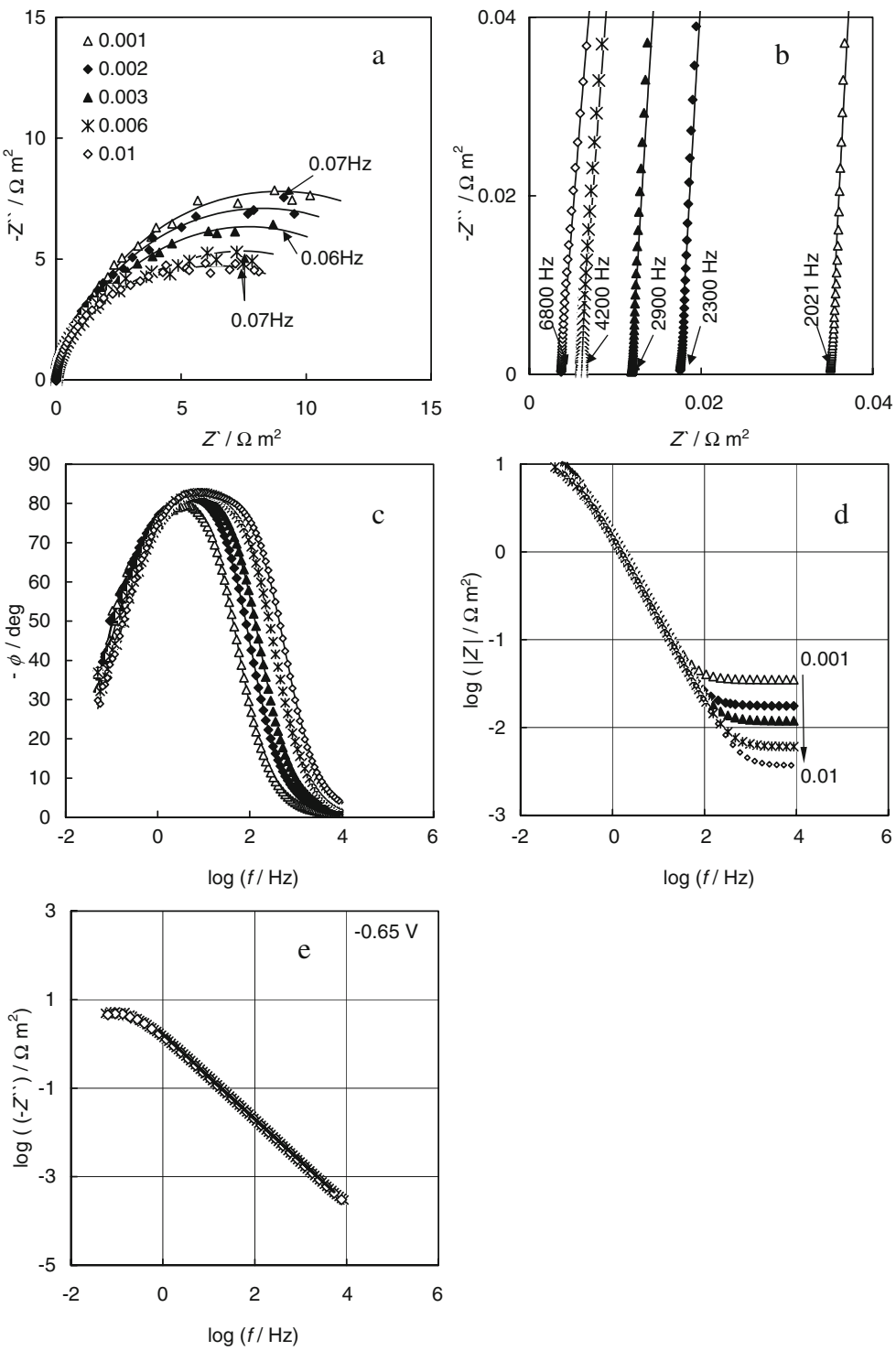

Fig. 1 Plots of EIS spectra of EP Bi(001) at ν=150 rpm and at the electrode potential E= −0.65 V in the case of $HClO_4$ aqueous solution with different concentrations (M; noted in figure), in various coordinates: Impedance complex plane plots ($-Z''$ vs. Z') (**a**), zoom of the high frequency part of plot **a** (**b**); phase angle (**c**), log $|Z|$ (**d**) and log($-Z''$) (**e**) vs. frequency dependences, (*symbols* experimental data, *solid lines* calculated data according to the circuit, given in Fig. 5)

($-Z''$) vs. log f plots are very helpful for the analysis of reaction characteristics, i.e., to obtain the characteristic relaxation time(s) of low-frequency process(es), as well as for CPE analysis of Bi(001) and other solid electrodes [18, 39–44, 46–53]. As can be seen in Figs. 1, 2 and 3, an almost capacitive–resistive behavior is observed at medium frequency region. For all concentrations studied (Figs. 1d, 2d, and 3d), the log $|Z|$ vs. log f dependences show an almost resistive response at higher frequencies f>1,000 Hz. The values of log $|Z|$, given in Figs. 1d, 2d, and 3d, are independent of electrode potential at frequency f>1×10^3 Hz, thus, there is no very quick faradaic processes at the Bi(001)|$HClO_4$+H_2O interface. At very high frequency, the values of active resistance $R_{el}=Z(\omega\rightarrow\infty)$ depend

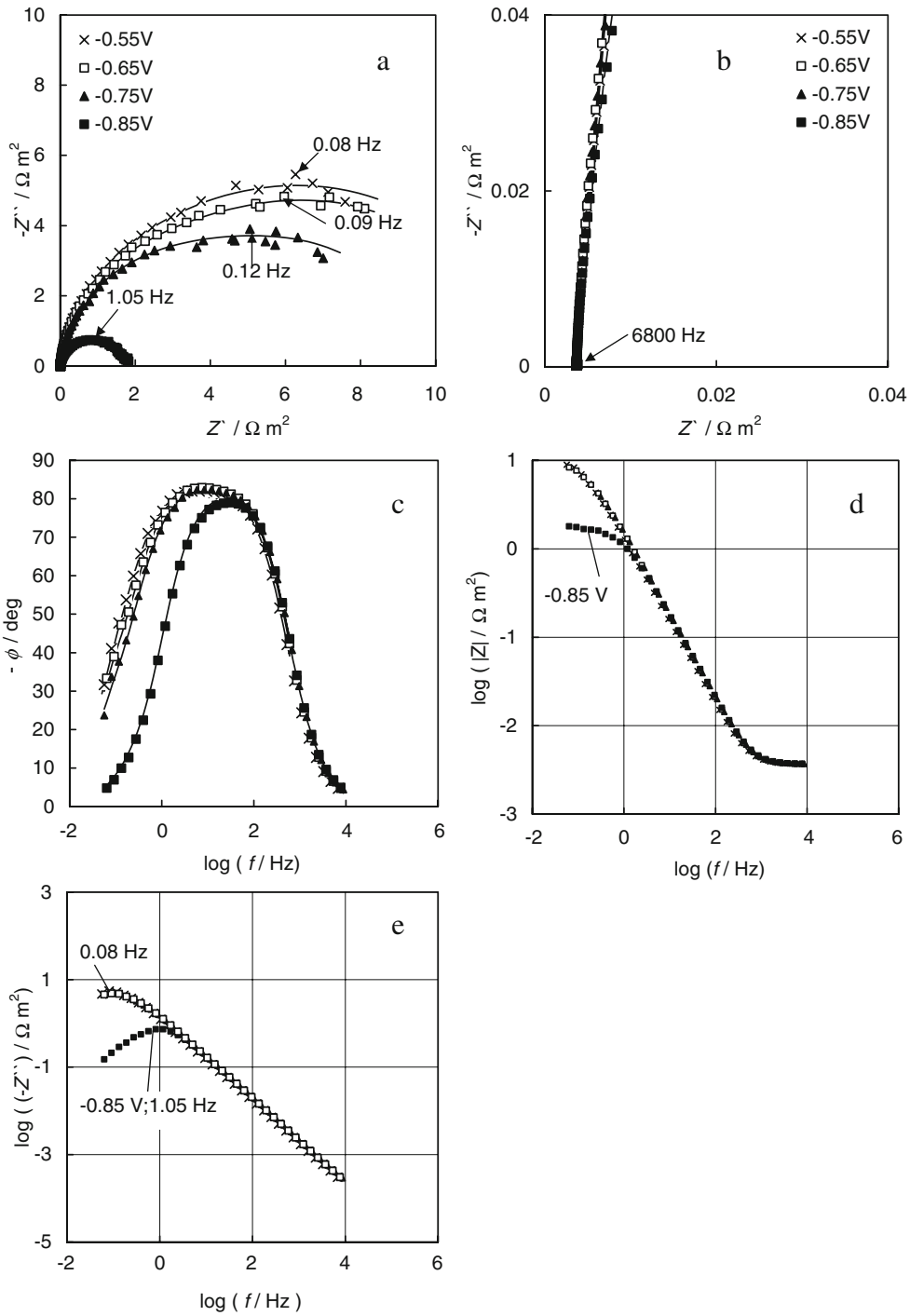

Fig. 2 Plots of EIS spectra of EP Bi(001) at ν=150 rpm in the 0.01 M $HClO_4$ aqueous solution at different electrode potentials (V; noted in figure), in various coordinates: Impedance complex plane plots ($-Z''$ vs. Z') (**a**); zoom of the high frequency part of plot **a** (**b**), phase angle (**c**), log $|Z|$ (**d**) and log ($-Z''$) (**e**) vs. log f dependences, (*symbols* experimental data, *solid lines* calculated data according to the circuit in Fig. 5)

nearly linearly on c_{HClO_4}, explained by the increase of the specific conductivity of the electrolyte resistance R_{el} with the rise of c_{HClO_4}.

The data in Figs. 1e, 2e and 3e show that for dilute $HClO_4$ solutions ($c_{HClO_4} \leq 1 \times 10^{-3}$M) at small negative electrode potentials, the log($-Z''$) vs. log f plots have not-very-well-expressed maxima even at very low f and, thus, the values of characteristic relaxation time $\tau_{max}=(2\pi f_{max})^{-1}$ (f_{max} is the frequency at the maximum of the ($-Z''$) vs. Z' plots) can not be calculated exactly, indicating the occurrence of very slow kinetic process(es) at the Bi(001) surface. The values of total polarization resistance R_p ($\omega \rightarrow 0$) at the electrode potentials E less negative than −0.75 V can not be determined exactly (Figs. 1a, 2a, and 3a) and only at $E \leq -0.80$ V is it possible to calculate the values of R_p ($\omega \rightarrow 0$), depending on c_{HClO_4}. For solutions with $c_{HClO_4} \geq 2 \times 10^{-3}$M, the values of τ_{max} obtained (given in Fig. 4) depend on the electrode potential applied.

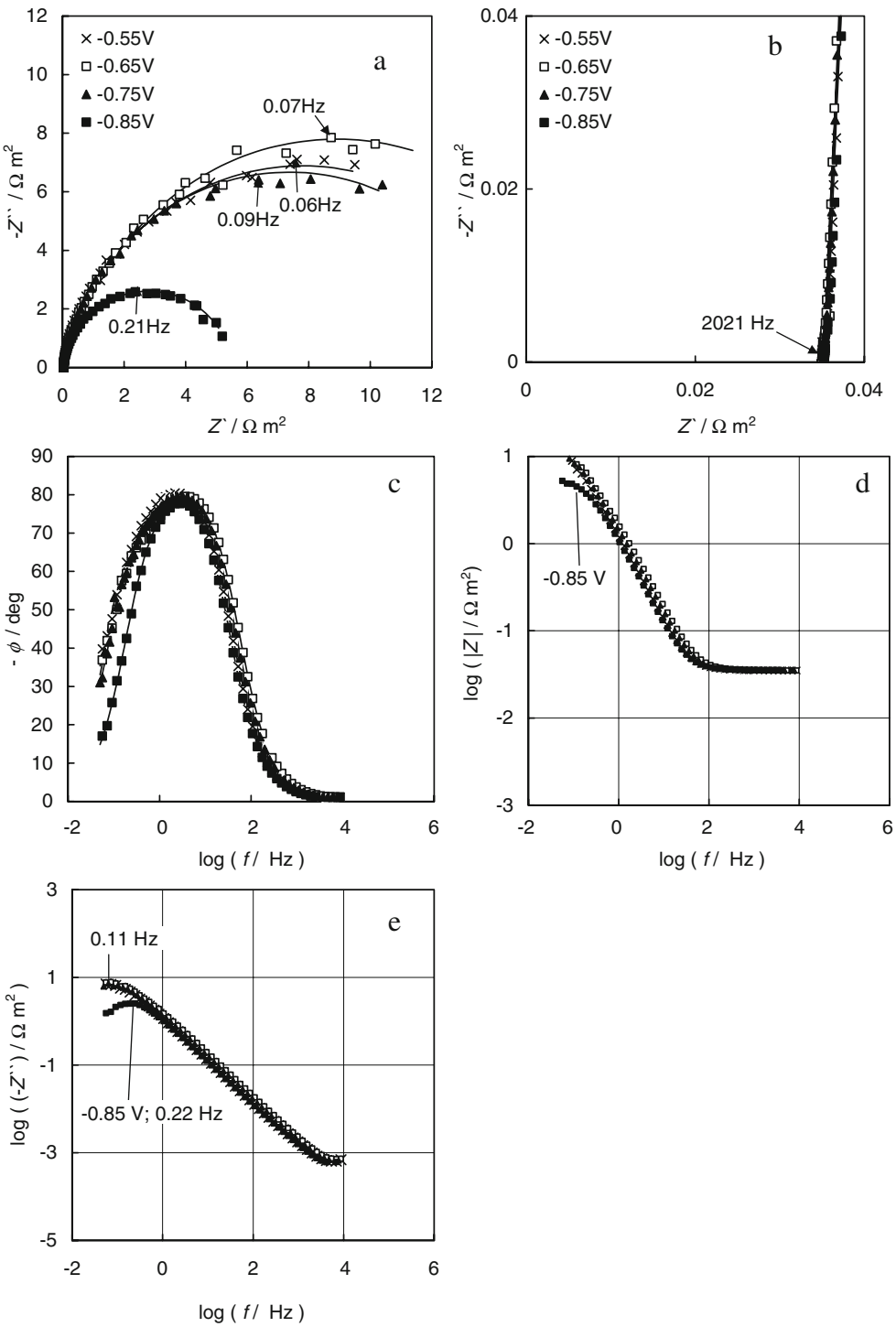

Fig. 3 Plots of EIS spectra of EP Bi(001) at ν=150 rpm in the 0.001 M $HClO_4$ aqueous solution at different electrode potentials (V; noted in figure), in various coordinates: Impedance complex plane plots ($-Z''$ vs. Z') (**a**); zoom of the high frequency part of plot **a** (**b**), phase angle (**c**), log $|Z|$ (**d**) and log ($-Z''$) (**e**) vs. log f dependences, (*symbols*—experimental data, *solid lines*—calculated data according to the circuit in Fig. 5)

According to the data given in Figs. 1, 2 and 3, the total polarization resistance decreases with increasing negative electrode potential as well as c_{HClO_4}, (i.e. with the decrease of pH). The values of τ_{max} in Fig. 4, obtained using data in Figs. 1e, 2e and 3e, are in a good agreement with τ_{max}, obtained from impedance complex plane plots (Figs. 1a, 2a and 3a). τ_{max} is practically independent of c_{HClO_4} at fixed potential if $E \geq -0.65$ V, but τ_{max} depends noticeably on E, if $c_{HClO_4} = \text{const}$.

In the region of frequency from 1 to 3×10^3 Hz, there is a noticeable dependence of log|Z| and phase angle ϕ values on log f, indicating the comparatively slow electrical double-layer formation process. In this region, ϕ noticeably depends on c_{HClO_4} and only very weakly on E (Figs. 1c, 2c

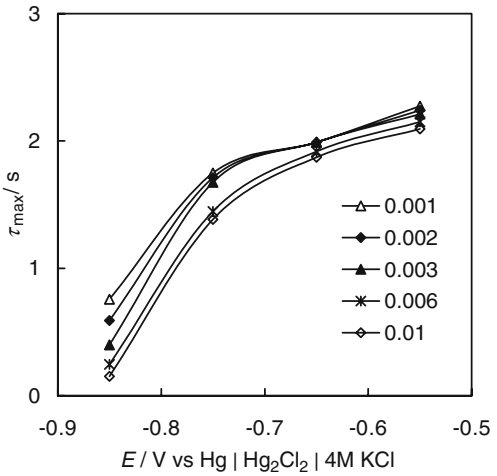

Fig. 4 Characteristic relaxation time $\tau_{max}=(2\pi f_{max})^{-1}$ vs. electrode potential dependences for cathodic hydrogen evolution at Bi(001) in $HClO_4$ aqueous solution with concentrations (M), noted in figure

and 3c). The analysis of ϕ vs. log f plots shows that, in the limited region of frequencies $1<f<100$ Hz, the very high negative values of phase angle, practically independent of electrode potential applied, have been observed, characteristic of the nearly ideally flat capacitive electrode, caused by the high values of resistances (R_{ad} and R_{ct}) values in parallel with the double-layer impedance. Only at very low frequency has the noticeable increase in absolute values of phase angle been observed indicating the occurrence of the very slow charge-transfer process (step) for HER at Bi(*hkl*). At a frequency $f>100$ Hz, the values of the phase angle are nearly independent of electrode potential applied. The influence of $c_{H_3O^+}$ on the position of the ϕ vs. log f plots is noticeable in the region of 100 Hz$<f<10^4$ Hz, and with the dilution of $HClO_4$ solution, ϕ vs. log f plot is shifted toward lower frequencies.

The analysis of the $\log(-Z'')$ vs. log f plots (Figs. 1e, 2e and 3e) shows that the deviation of the experimental system from the ideally flat surface toward constant phase element behavior is very small [18, 39–44, 46–50] because the fractional exponent α_{CPE} for CPE with impedance $Z_{CPE}=Q^{-1}(j\omega)^{-\alpha_{CPE}}$, calculated from the slope of $\log(-Z'')$ vs. log f plots, is only somewhat lower than unity ($0.94<\alpha_{CPE}<0.98$), thus characteristic of the ideally flat capacitive interface.

Fitting results of impedance data

The number of experimental points in the impedance spectra has been kept constant if the various ECs have been tested. The good fitting ($\chi^2<7\times10^{-4}$, SD$\leq2.7\times10^{-4}$, $\Delta^2\leq0.2$) at $c_{HClO_4}\leq 2\times10^{-3}$M has been established if EC (i.e., model with one adsorbed intermediate species [18, 43, 44], proposed by Armstrong and Henderson [44]), corresponding to the reaction steps given by Eqs. (2a) and (2b), has been applied. The very low SD values, calculated using the method described in [46], nearly independent of the electrode potential applied, have been obtained. According to the fitting results, the high-frequency series resistance at $c_{HClO_4}=$ const. is independent of potential applied and, thus, the calculated values of R_{el} correspond to the high-frequency electrolyte resistance. In the C_{dl} vs. E curves for solutions with $c_{HClO_4}\leq 2\times10^{-3}$M, there are characteristic diffuse layer minima at the diffuse layer minimum potential $E_{min}=-0.65$ V (Fig. 6a), being in a good agreement with the zero-charge potential $E_{\sigma=0}$ obtained for $LiClO_4$ solutions [24, 25], and, therefore, the C_{dl} vs. E curves for dilute $HClO_4$ solutions ($c_{HClO_4}<2\cdot10^{-3}$M) can be used for classical Frumkin ψ_1 potential correction analysis [24, 31, 35–38].

However, according to the detailed analysis in the case of solid electrodes [18, 24–26, 39–51], the CPE element should be included into EC and, therefore, the double-layer capacitance C_{dl} is valid for the ideally flat and energetically homogenous surface has to be replaced with CPE, taking into account the geometrical surface roughness and energetic inhomogeneity of solid surface studied, to receive EC given in Fig. 5. According to the data in Figs. 1, 2 and 3, a very good fit ($\chi^2<5\times10^{-4}$, $\Delta^2\leq0.01$) has been observed if the modified Armstrong–Henderson EC has been used (solid lines—calculated impedance spectra using the model in Fig. 5; symbols—the experimental data). The results (Fig. 6b) show that the Q depends very weakly on the electrolyte concentration and Q has minimal values in dilute $HClO_4$ solutions near $E_{min}=-0.65$ V, being in a very good agreement with C_{dl} values (Fig. 6a) obtained using Armstrong–Henderson EC. This is not surprising as the values of α_{CPE} at fixed E for dilute $HClO_4$ solutions are quite high ($\alpha_{CPE}\geq0.97$) and depend weakly on c_{HClO_4} if $c_{HClO_4}\leq 2\times10^{-3}$M. It should be mentioned that α_{CPE} decreases with the rise of c_{HClO_4} (Fig. 6c), contrary to the

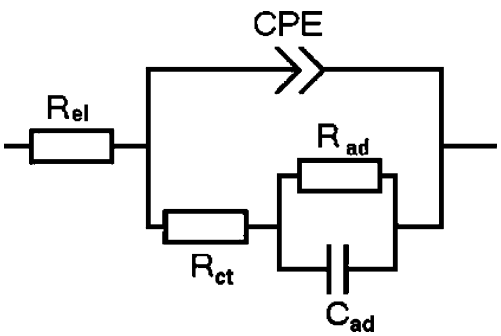

Fig. 5 Modified Armstrong–Henderson model [45], where C_{dl} has been replaced by CPE, taking into account the adsorption of one intermediate particle used for fitting the experimental results: (R_{el} high-frequency solution resistance, *CPE* constant phase element, R_{ct} charge-transfer resistance, R_{ad} adsorption or partial charge-transfer resistance, C_{ad} adsorption capacitance)

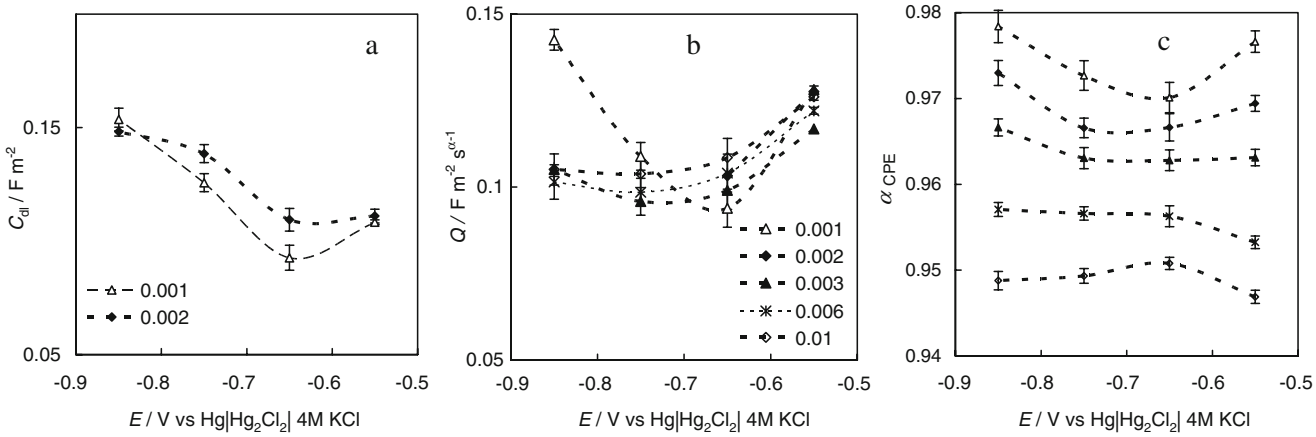

Fig. 6 Dependences of C_{dl} (**a**; calculated according to the Armstrong–Henderson circuit); CPE coefficient Q (**b**) and fractional exponent α_{CPE} (**c**) on the electrode potential (calculated according to the circuit in Fig. 5) for EP Bi(001) in $HClO_4$ aqueous solution with concentrations (M), noted in figure

Bi(001)|$LiClO_4$+H_2O system, where α_{CPE} increases with the rise of c_{LiClO_4} [1, 24, 25]. Moreover, differently from $LiClO_4$ solutions, there is a very small minimum in the α_{CPE} vs. E dependence at E=−0.65 V. The dependence of α_{CPE} on $c_{HClO_4} > 4 \times 10^{-3}$M indicates the very weak changes in surface energetic inhomogeneity caused by the adsorption of reaction intermediates. However, $\alpha_{CPE} \geq 0.97$ for 1×10^{-3} M $HClO_4$ aqueous solution indicates that the deviation of Bi(001)|$HClO_4$ interface from the classical conception of ideally flat interface [24, 25, 49, 50] is very weak and the influence of replacing CPE with C_{dl} in EC on the values of other fitting parameters is comparatively small. At these conditions, to a first very rough approximation, the model of Brug et al. [47] can be used for calculation of the ideal C_{dl} values (Fig. 6a). This result can be explained by the fact that α_{CPE} for solutions with higher $c_{HClO_4} (\geq 2 \times 10^{-3}\text{M})$ contains additional information concerning the influence of the weakly blocking adsorption of electrolyte ions and hydrogen on Bi(001), but not simply the surface roughness effect [24–26, 41].

According to the data (Fig. 7a), the charge-transfer resistance decreases noticeably with an increase in the negative electrode potential, and R_{ct} is practically independent of c_{HClO_4} at E_{min}=−0.65 V, where the values of C_{dl} or Q are minimal [34, Härk and Lust 2008, in preparation].

The calculated values for double layer corrected current density $j_{sum} = \frac{RT}{nF(R_{ct}+R_{ad})} = (2.13 \pm 0.01) \times 10^{-6}$A cm^{-2} at $E_{\sigma=0}$ (n is the number of electrons transferred) are in good agreement with those obtained from the stationary Tafel measurements ($j_{ct}=2\times10^{-6}$A cm^{-2} for 0.1 M $HClO_4$) [1]. At $E>E_{min}$, there is only a small decrease of R_{ct} with the rise of c_{HClO_4} caused by less-pronounced classical Frumkin ψ_1 potential effect [1, 34–38, Härk and Lust 2008, in preparation]. The adsorption resistance, R_{ad} (Fig. 7b), depends noticeably on the electrode potential, being maximal near the E_{min} and the values of R_{ad} have a

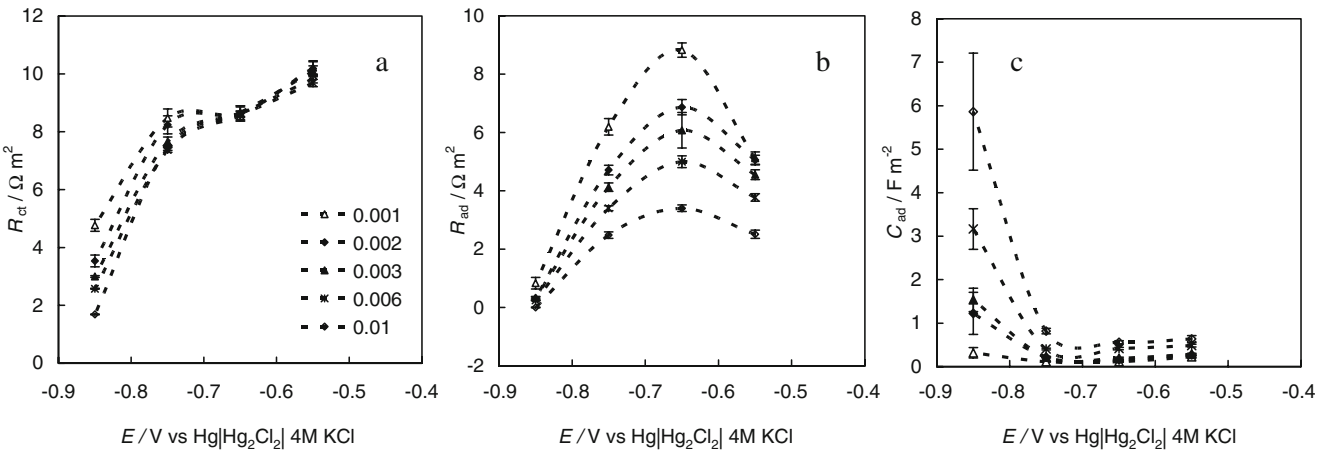

Fig. 7 R_{ct} (**a**); R_{ad} (**b**) and C_{ad} (**c**) dependences on the electrode potential (calculated according to the equivalent circuit in Fig. 5) for EP Bi(001) in $HClO_4$ aqueous solution with different concentrations (M), noted in figure

noticeable decrease with the rise of negative E. The decrease of R_{ad} with c_{HClO_4} is pronounced only in the region of small positive surface charge densities. The adsorption capacitance, C_{ad} (Fig. 7c), is nearly independent of E and c_{HClO_4} at $E>-0.7$ V. At more negative potentials, C_{ad} noticeably increases, which is more expressed for solutions with lower pH. In concentrated $HClO_4$ solutions, C_{ad} is nearly 60 times higher than the values of Q at $E=-0.85$ V (Fig. 7c), indicating that the hydrogen adsorption is practically impossible at Bi(001) surface.

The attempts to use more complicated models like the Ershler model (nowadays known as Frumkin–Melik–Gaikazyan–Randles circuit [41, 43]) or the modified Grafov–Damaskin ECs, based on the multi-port impedance model for totally irreversible reaction discussed in detail in [51, 52], did not give a better fit for the experimental data and the errors in R_{ad} and C_{ad} are very high. Thus, a modified Armstrong–Henderson model (Fig. 5) is the only EC giving a good fit of the Bi(001)|$HClO_4$+H_2O interface data.

The so-called corrected Tafel plots (cTp) have been calculated according to the Eq. (4):

$$\log\, j + zF\psi_1(2.3\mathrm{RT})^{-1} = \text{const.} + (1-\alpha)\log c + \alpha nF(2.3\mathrm{RT})^{-1}(E - E_{\sigma=0} - \psi_1) \quad (4)$$

where α is a transfer coefficient, z is charge number of particle, and n is the number of electrons consumed [1]. For calculation of the cTp, ψ_1 potential has been taken equal to ψ_0 potential ($\psi_1 \approx \psi_0$), i.e., the reaction center has been taken to locate at the outer Helmholtz plane with the ψ_0 potential. The needful ψ_0 vs. E and surface charge density σ vs. E plots have been calculated using corresponding impedance data obtained for less concentrated $HClO_4$ solutions $c_{HClO_4} < 2\times10^{-3}$M, where the influence of hydrogen adsorption on the values of C_{dl} or Q is weak. Calculated cTps are nearly linear for more concentrated $HClO_4$ solutions ($c_{HClO_4} > 6\times10^{-3}$M) and corrected values of current density are nearly independent of c_{HClO_4} at $E - E_{\sigma=0} - \psi_0 < 0$. Thus, the cTps analysis method can be used for Bi(001)|$HClO_4$ interface data (Fig. 8), similarly to the systems with constant ionic strength [1, 31, 36]. It was found that the slope of cTp is equal to 0.117 V, giving the value of α equal to 0.51, in a good agreement with the data for Bi(*hkl*)|constant ionic strength electrolyte interface [1]. If the corrected Tafel plots can be taken as representative of the kinetic mechanism [29, 31–33, 35–38] then, in a good agreement with the impedance data, the slow primary discharge is the slowest rate determining step. Of course, the same slope value would be observed for slow electrochemical desorption (Heyrovsky), i.e., $H_3O^+ + M H_{ad} + e^- \rightarrow H_2 + H_2O + M$ step, but then the surface coverage of Bi(001) with adsorbed H_{ad} should be very high (and therefore $\theta_{H_{ads}} \rightarrow 1$), that is impossible in the case of Bi (001) [1, 38, Härk and Lust 2008, in preparation] based on the data in Fig. 7c. The electroreduction reaction of H_3O^+ cations at the Bi(001)|$HClO_4$+H_2O interface is mainly limited by the very slow charge-transfer step and moderate rate of electrical double-layer formation process, i.e., by the adsorption of solvent molecules, hydrated cations and anions at Bi(001) surface near the zero-charge potential, based on the data in Figs. 1, 2, 3 and 4.

Conclusions

Electrochemical impedance spectroscopy has been applied for investigation of the hydrogen evolution kinetics at the electrochemically polished Bi(001) plane. The mixed kinetics reaction mechanism (slow adsorption and charge-transfer steps) has been established for cathodic hydrogen evolution at Bi(001)|$HClO_4$+H_2O interface. The charge-

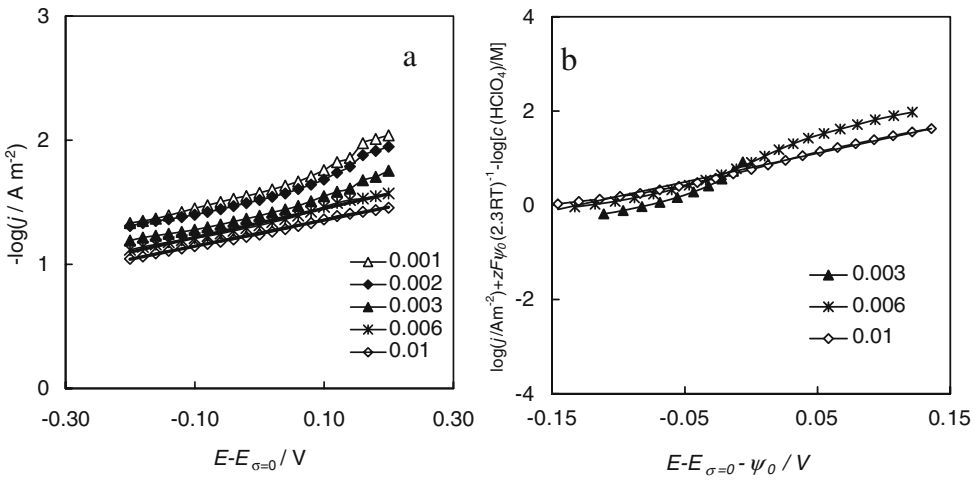

Fig. 8 $-\log j$ vs. rational electrode potential $(E - E_{\sigma=0})$ plots (**a**) and corrected Tafel plots (**b**) for EP Bi(001) in $HClO_4$ aqueous solution with concentrations (M), noted in figure

transfer resistance, R_{ct}, and adsorption capacitance, C_{ad}, depend noticeably on the electrode potential applied. The double-layer corrected current density values, calculated from the impedance data at zero-charge potential, are in good agreement with those obtained using stationary polarization method. The adsorption resistance R_{ad} value is maximal in the region of zero-charge potential. The fractional exponent of the constant phase element CPE $(\alpha_{CPE} \geq 0.94)$ only very weakly depends on the $HClO_4$ concentration and electrode potential, and therefore, the deviation of $Bi(001)|HClO_4+H_2O$ interface from the classical conception of ideally flat electrode is weak and CPE coefficient Q is nearly equal to the high-frequency electrical double-layer capacitance C_{dl}, if $(\alpha_{CPE} \geq 0.94)$. Similar to the stationary polarization measurements, the electrical double-layer structure, determining the ψ_1 (or ψ_0) potential values, depending strongly on the effective Debye screening length of the electrolyte ions, has a very big influence on the cathodic hydrogen evolution kinetics at the Bi(001) plane from $HClO_4$ aqueous with variable pH of solution.

Acknowledgment This work was supported in part by the Estonian Science Foundation under Project Nos. 6696 and 5803.

References

1. Lust K, Perkson E, Lust E (2000) Russ J Electrochem 36:1257
2. Lasia A, Rami A (1990) J Electroanal Chem 294:123
3. Clavilier J, Rodes A, El Achi K, Zamarhchari MA (1991) J Chem Phys 88:1291
4. Morin S, Dumont H, Conway BE (1996) J Electroanal Chem 412:39
5. Lucas CA, Marković NM (2003) In: Bard AJ, Stratmann M (ed) Encyclopedia of electrochem, vol 2. Wiley VCH, p 291
6. Bai L, Conway BE (1986) Electrochim Acta 32:1013
7. Schönfuss D, Müller L (1994) Electrochim Acta 39:2097
8. Harrington DA, Conway BE (1987) Electrochim Acta 32:1703
9. Breiter MW (1961) In: Yeager E (ed) Symposium on electrode processes. The Electrochemical Society. Wiley, New York, p 307
10. Seto K, Ianelli A, Love B, Lipkowski J (1987) J Electroanal Chem 226:351
11. Marković NM, Sarkaf ST, Gasteiger HA, Ross PN Jr (1996) J Chem Soc, Faraday Trans 92:3719
12. Breiter MW (1962) J Electrochem Soc 109:549
13. Losev VV (1981) Elektrokhimija 17:733
14. Duncan H, Lasia A (2007) Electrochim Acta 52:6195
15. Lim C, Pyun S-I (1993) Electrochim Acta 38:2695
16. Lasia A, Grégoire D (1995) J Electrochem Soc 142:3393
17. Chen JS, Diard J-P, Durand R, Montella C (1996) J Electroanal Chem 406:1
18. Lasia A (1999) In: Conway BE, Bockris JO'M, White RE (eds) Modern aspects of electrochemistry, vol 32. Kluwer/Plenum, New York, p 143
19. Lasia A (2006) J Electroanal Chem 593:159
20. Horvat-Radošević V, Kvastek K (2002) Electrochim Acta 48:311
21. Montella C (2000) J Electroanal Chem 480:150
22. Langkau T, Baltruschat H (1998) Electrochim Acta 44:909
23. Arold J, Tamm J (1989) Elektrokhimija 25:1417
24. Trasatti S, Lust E (1999) In: White RE, Conway BE, Bockris JO'M (eds) Modern aspects of electrochemistry, vol 33. Kluwer/Plenum, New York, p 1
25. Lust E (2002) In: Bard AJ, Stratmann M (ed) Encyclopedia of electrochemistry, vol 1. Wiley, p 188
26. Brug GJ, Sluyters-Rehbach M, Sluyters JH, Hemelin A (1984) J Electroanal Chem 181:245
27. Eberhardt D, Santos E, Schmickler W (1999) J Electroanal Chem 461:76
28. Jović VD, Parsons R, Jović BM (1992) J Electroanal Chem 339:327
29. Doubova LM, Trasatti S (1999) J Electroanal Chem 467:164
30. El-Halim AMAbd, Jüttner K, Lorenz WJ (1980) J Electroanal Chem 106:193
31. Trasatti S (1997) In: Gerischer H, Tobias CW (eds) Advances in electrochemistry and electrochemical engineering, vol 10. Wiley, New York, p 123
32. Kolb DM (1993) In: Lipkowski J, Ross PN (eds) Structure of electrified interfaces. VCH, New York, p 65
33. Hamelin A (1995) In: Gewirth AA, Siegenthaler H (eds) Nanoscale probes of the solid|liquid interface. Kluwer, Dordrecht, p 285
34. Jäger R, Härk E, Möller P, Nerut J, Lust K, Lust E (2004) J Electroanal Chem 566:217
35. Frumkin AN (1961) In: Delahay P (ed) Ads Electrochem Sci Electrochem Eng, vol 1. Wiley, New York, p 1
36. Petrii OA, Nazmutdinov RR, Bronshtein MD, Tsirlina GA (2007) Electrochim Acta 52:3493
37. Gileadi E, Kirowa-Eisner E (2005) Corros Sci 47:3068
38. Palm U, Tenno T (1973) J Electroanal Chem 42:457
39. Orazem ME, Pèbère N, Tribollet B (2006) J Electrochem Soc 153: B129
40. Huang VM-W, Vivier V, Pèbère N, Orazem ME, Tribollet B (2007) J Electrochem Soc 154:C81
41. Thomberg T, Nerut J, Lust E (2006) J Electroanal Chem 586:237
42. Macdonald JR (ed) (1987) Impedance spectroscopy: emphasizing solid materials and systems. Wiley, New York
43. Lasia A (2002) In: Conway BE, White RE (eds) Modern aspects of electrochemistry, vol 35. Kluwer/Plenum, New York, p 1
44. Armstrong RD, Henderson M (1972) J Electroanal Chem 39:81
45. Zview for Windows (version 2.7) Fitting Program, Scribner, Southern Pines, NC, USA
46. Zoltowski P (2005) Solid State Ionics 176:1979
47. Brug GJ, Van der Eeden ALG, Sluyters-Rehbach M, Sluyters JH (1984) J Electroanal Chem 176:275
48. de Levie R (1989) J Electroanal Chem 261:1
49. Zoltowski P (1998) J Electroanal Chem 443:149
50. Kerner Z, Pajkossy T (1998) J Electroanal Chem 448:139
51. Pajkossy T, Wandlowski Th, Kolb DM (1996) J Electroanal Chem 414:209
52. Stoynov ZB, Grafov BM, Savova-Stoynova BS, Elkin VV (1991) Electrochemical impedance. Nauka, Moscow
53. Grafov BM, Damaskin BB (1994) J Electroanal Chem 366:29